JOURNAL OF AIRCRAFT
Vol. 41, No. 2, March–April 2004

Alleviation of Vertical Tail Buffeting of F/A-18 Aircraft

Essam F. Sheta*
CFD Research Corporation, Huntsville, Alabama 35805

A high-fidelity multidisciplinary computational investigation for the prediction of buffet characteristics and buffet alleviation of the vertical tail of full F/A-18 aircraft is conducted and presented. Alleviation of the vertical tail buffeting is achieved using streamwise wing fences. The problem is solved using four sets of high-fidelity analysis modules. The Reynolds-averaged full Navier–Stokes equations are solved for the aerodynamic flowfield. The structural dynamic responses of the vertical tail are computed using direct finite element analysis. The fluid–structure interfacing is modeled using conservative and consistent interfacing module. A transfinite interpolation algorithm is used to deform the computational grid dynamically to accommodate the deformed shape of the vertical tail. The investigation is conducted over a wide range of high angles of attack at a Mach number of 0.243 and a Reynolds number of 11×10^6. The LEX fences shift the onset of maximum buffet condition to higher angles of attack. The LEX fences also reduce the root-mean-square values of differential pressure and root bending moment. At 30-deg angle of attack, the acceleration power of the vertical tail tip is reduced by up to 38% at first bending mode and by up to 24% at first torsion mode. However, the effectiveness of the LEX fences for buffet alleviation is reduced for very high angles of attack.

Nomenclature

A_t = reference area of vertical tail, 4.842 m^2
C_P = coefficient of pressure, $(P - P_\infty)/q_\infty$
C_{rbm} = root bending moment coefficient, $M_B/q_\infty A_t \bar{C}$
$\bar{C}$ = mean aerodynamic chord of the wing, 3.5 m
$\bar{C}_P$ = mean pressure coefficient,

$$\left[\frac{1}{N}\sum_{1}^{N} C_P\right]$$

$\hat{C}_P$ = rms pressure coefficient,

$$\left[\frac{1}{N}\sum_{1}^{N} (C_P - \bar{C}_P)^2\right]^{\frac{1}{2}}$$

$F(n)$ = dimensionless buffet pressure power spectral density
$\hat{\boldsymbol{F}}_i$ = inviscid flux vector
$\hat{\boldsymbol{F}}_v$ = viscous flux vector
f = frequency, Hz
M_B = vertical tail root bending moment
N = number of sample points
n = nondimensional frequency, $f\bar{C}/U_\infty$
P_i = pressure on inboard tail surface
P_o = pressure on outboard tail surface
$\hat{\boldsymbol{Q}}$ = vector of conservative variables
q_∞ = freestream dynamic pressure
U_∞ = freestream velocity
α = angle of attack
ΔP = differential pressure, $P_i - P_o$

Introduction

VERTICAL tail buffeting is a serious problem that limits the ability of fighter aircraft to maneuver at high angles of attack. In fighter aircraft, such as the F/A-18, the leading-edge extension (LEX) of the wing maintains lift at high angles of attack by generating a pair of vortices that trails downstream over the aircraft. The vortices also entrain air over the vertical tails to maintain stability of the aircraft. However, at some flight conditions, the cores of the LEX vortices burst upstream of the vertical tail. The resulting turbulent flow impinges upon the vertical tail surfaces causing severe structural vibrations and premature failure of the vertical tail.

The F/A-18 aircraft, in particular, was the subject of numerous research works to identify the buffet characteristics of the vertical tails. The experimental studies of Wentz,[1] Sellers et al.,[2] Lee and Brown,[3] Cole et al.,[4] Martin and Thompson,[5] and Moses and Pendleton[6] revealed that the LEX vortices burst ahead of the vertical tail at angles of attack of 25 deg and higher. At high angles of attack, the buffet pressure concentrates in a narrow, low-frequency band. The buffet response occurs in the first bending mode, increases with increasing dynamic pressure, and is larger at Mach numbers of approximately 0.3 than at higher Mach numbers. The bending mode response is strongly coupled with the characteristic frequency of the buffet flow. Bean and Lee[7] conducted wind-tunnel experiments on a rigid 6% scale model of the F/A-18 aircraft over a wide range of angles of attack. They found that tail buffeting in the fundamental torsional mode occurred at lower angles of attack with larger buffet magnitude compared to those of the fundamental bending mode. The problem of vertical tail buffeting was also observed on several modern fighter aircraft. For example, Moses and Huttsell[8] have shown that buffet characteristics of an early F-22 aircraft model are similar to characteristics observed on the F/A-18 aircraft.

Computationally, there have been limited successes in analyzing the buffet problem. Rizk et al.[9,10] solved the Reynolds-averaged, thin-layer Navier–Stokes equations around the F/A-18 aircraft at $\alpha = 30$ deg. A chimera embedded grid consisting of 0.9 million cells was used to model the symmetric half of the aircraft. The aerodynamic results were qualitatively similar to some experimental data. Later, Gee et al.[11] used 1.7 million cells to capture more robust vortices. A weak coupling between the aerodynamics and structures was considered by assuming rigid tails. Thus, the inertial effects of the acceleration of the tail points on the flowfield were neglected, which reduces the accuracy of the results. They concluded that the dominant frequency was very close to the first natural frequency of the tail. The time history showed a pattern of near periodic fluctuations of the loads. Sheta et al.[12] and Sheta and Huttsell[13] used a high-fidelity method to investigate the buffet characteristics of the vertical tail of a full F/A-18 aircraft model. The investigation emphasized the significance of strong coupling between the fluid and structure. The results compared well with several sets of experimental data.

Received 15 July 2002; presented as Paper 2003-1888 at the AIAA 44th SDM Conference, Norfolk, VA, 7–10 April 2003; revision received 3 June 2003; accepted for publication 14 June 2003.

*Senior Engineer, Aeromechanics Division, 215 Wynn Drive. Senior Member AIAA.

Several attempts have been made to alleviate tail buffeting. Rao et al.[14] proposed two concepts for buffet alleviation at high angles of attack. The first concept was a passive dorsal fin extension to the vertical tails. The dorsal fin had a highly swept leading edge for generating counter-rotating vortex that was induced below the LEX vortices. The fin extension restructured the post-breakdown flow before its encounter with the tail surface, resulting in alleviation of the tail buffet loads. However, the magnitude of lift loss due to the fin extension outweighed the effect of delayed vortex breakdown. The magnitude of the lift loss was directly related to the size of the dorsal fin. The second concept was an up-deflected LEX, which reduced the tail buffeting with some loss in the maximum lift. The directional stability of the aircraft was also reduced by the up-deflected LEX. Shah[15] conducted extensive wind-tunnel studies on the impact of LEX modifications (including reduced LEX chord, reduced LEX span, LEX fence, and removal of the LEX) on the buffet characteristics of a 16%-scale model of the F/A-18 aircraft. The results indicated that the aerodynamic and buffet characteristics were strongly dependent on the LEX geometry, which influenced the strength, position, and bursting of the vortices. The reduced chord LEX caused a reduction in the maximum lift and substantial nose-down pitching moment. The reduced span LEX produced a more stable vortex and delayed the vortex breakdown. However, a loss of 3% in the maximum lift and a significant nose-down pitching moment was observed.

The LEX fence (the only method to be actually used on the real aircraft for buffet alleviation) was developed through trial and error in the wind tunnel and validated in flight. The LEX fences were fitted over the upper surface of the wing LEX near the leading edge of the wing.[15–18] The LEX fences modified the vortical flow upstream of the vertical tail and reduced tail buffeting. In the flight data reported by Lee et al.,[16] the acceleration peaks at a point close to the tip of the vertical tail were reduced from 450 to 200 g with the addition of the LEX fence. A loss of 3% of maximum lift was seen because the fence disrupts the basic vortical flow. The fences were also less effective at high angles of attack.

In this investigation, time-accurate, high-fidelity, multidisciplinary numerical analysis for prediction and alleviation of vertical tail buffeting of full F/A-18 aircraft at typical flight conditions is presented. The results of the basic configuration of the F/A-18 aircraft are compared with the LEX-on configuration over a wide range of high angles of attack. The results of this investigation are extensively validated using several experimental and flight-test data.

Technical Approach

The tail buffet problem is a complex multidisciplinary aeroelastic phenomenon that involves interaction between several physical disciplines. The physical disciplines are the fluid dynamics of the flowfield and the structural dynamics of the flexible surfaces. Other numerical disciplines that are related to computation of the solution, such as the grid deformation and the fluid–structure interface coupling, are also involved. The modules of these multidisciplinary disciplines are integrated into the multidisciplinary computing environment (MDICE).[19] MDICE enables the multidisciplinary analysis modules to run concurrently and cooperatively on a distributed network of computers to perform the analysis. The particular sets of analysis modules used in the current investigation are outlined next.

Fluid Dynamics Module

The buffet problem of vertical tails occurs at high angles of attack where the flowfield is characterized by strong vortical flow and massive three-dimensional flow separation; see Sheta.[20] Therefore, the problem mandates the solution of the full Navier–Stokes equations to account for vorticity evolution, convection, shedding, vortex bursting, and strong fluid–structure interactions. Euler and thin-layer Navier–Stokes equations can give an approximate solution in the region of primary vortices, but they cannot model the three-dimensional viscous effects or predict the accurate location and strength of the secondary and tertiary vortices.

In this investigation, the flowfield is represented by the integral form of the Reynolds-averaged full Navier–Stokes equations,

$$\iiint_V \frac{\partial \hat{\boldsymbol{Q}}}{\partial t}\,\mathrm{d}V + \oint\!\!\int_S (\hat{\boldsymbol{F}}_i - \hat{\boldsymbol{F}}_v)\cdot \hat{n}\,\mathrm{d}S = 0 \tag{1}$$

The integral form of the equations is modified to account for the effect of the moving volume (due to the flexibility of the vertical tails) as follows:

$$\iiint_V \frac{\partial \hat{\boldsymbol{Q}}}{\partial t}\,\mathrm{d}V + \oint\!\!\int_S (\hat{\boldsymbol{F}}_i - \hat{\boldsymbol{F}}_v - \hat{\boldsymbol{Q}}\,\bar{v}_g)\cdot \hat{n}\,\mathrm{d}S = 0 \tag{2}$$

where $\bar{v}_g$ is the volume surface velocity, $\hat{n}$ is the normal to the volume surface, and S is the surface area. If the control volume V is fixed is space, then $\bar{v}_g = 0$. The equations are solved using an implicit finite volume upwind scheme with Roe's flux-difference splitting for spatial differencing and a fully implicit upwind scheme for temporal differencing.

Initial and Boundary Conditions

Initially, freestream conditions are assumed everywhere. The flowfield characteristics are then computed assuming a rigid configuration. The computations continue until the changes in the flowfield solution become insignificant. The final solution is then used as the initial conditions for the next step. The physical boundary conditions assume Riemann's inflow/outflow boundary conditions at the far-field boundaries in all directions. On the aircraft surfaces, the no-slip and no-penetration conditions are enforced. That is, the relative velocity equals to zero. The normal pressure gradient equals to zero on stationary surfaces. On the vibrating tail surfaces, the normal pressure gradient is no longer zero due to the inertia of the moving tail. The pressure gradient on the vibrating surfaces becomes $\partial p/\partial \hat{n} = -\rho(\vec{a}\cdot\hat{n})$, where $\vec{a}$ is the acceleration of a point on the accelerating surface and $\hat{n}$ is the unit normal. At the grid interface boundaries, the solution is interpolated across the boundaries using conservative interpolation. Conservative interpolation seeks to conserve the forces and moments between two adjacent cells. Because of the symmetry of the F/A-18 aircraft, only half the aircraft is considered, and the symmetry boundary condition is assumed at the symmetry boundary. The experimental observations of Pettit et al.[21] indicate that responses of starboard and port tails of the F/A-18 aircraft are similar at zero sideslip. The cases considered in the current investigation are all set at zero sideslip. Therefore, symmetric boundary conditions are considered sufficient.

Structure Dynamics Module

The structural dynamic response of the vertical tail is analyzed using three-dimensional direct finite element analysis. It is assumed that the vertical tail is the only flexible structure in the aircraft. The initial condition is the undeformed vertical tail. The root of the vertical tail is assumed clamped. No structural damping is assumed in this investigation. The unsteady aerodynamic forces are projected on the surfaces of the vertical tail structure and, consequently, into the finite element equations, from the fluid dynamics model. The vertical tail of the F/A-18 aircraft is modeled using second-order hexahedral elements.

Fluid–Structure Interfacing Module

The fluid–structure interface algorithm is used to project the forces and moments from the fluid flow to the flexible-body structure and to feed back the aeroelastic deflections of the structure to the flow field. The interfacing is formulated in the most general sense for maximum flexibility. There is no inherent assumption that the fluids grid is matched with the structure grid, either through different mesh densities, mesh architecture, or through physical separation between the interfaces, as seen with thick-shell finite element models. The current simulation uses a conservative and consistent interface, adapted from Brown.[22] Conservative interfaces aim to conserve the forces and moments in the interpolation process between

two grids. In this case, the sum of all forces and moments on the fluid interface is equivalent to the sum of all forces and moments on the structure interface. Consistency, or virtual work conservation, requires that the virtual work performed by the solid interface is equivalent to the virtual work performed by the fluid interface.

Grid Deformation Module

The computational grid is deformed every fluid–structure data transfer to accommodate the deformed shape of the tail. The six outer boundary surfaces of the deformed grid block are kept fixed. The grid is deformed using a transfinite interpolation algorithm (TFI). The advantages of using TFI are that TFI is an interpolation procedure that deforms grids conforming to specified boundaries and it is very computationally efficient. The spacing between points in the physical domain is controlled by blending functions that specify how far into the original grid the effect of the new position of the flexible body surfaces is carried. The grid points on the surface of the tail are moving with the deflections of the tail. The deformation of the grid points decreases as you go far from the boundary in all directions and vanishes at the outer boundary of the deformed block. The TFI routine is invoked automatically when a fluid–structure interface is exchanged between application modules.

Multidisciplinary Computing Environment

The multidisciplinary modules used in the current investigation are integrated into MDICE; see Kingsley et al.[19] MDICE is a distributed object-oriented environment for parallel execution of multidisciplinary modules. Using the MDICE environment, one can avoid giant monolithic codes that attempt to provide all modules in a single large computer program. Such large programs are difficult to develop and maintain and by their nature cannot contain up-to-date technology. MDICE allows the reuse of existing, state-of-the-art codes that have been validated. The flexibility of exchanging one application program for another enables each engineer to select and apply the technology best suited to the task at hand. MDICE increases the computational efficiency by utilizing a parallel-distributed heterogeneous network of computers. Additional analysis modules can be integrated into the environment without modifying or breaking the modules already in the environment.

Configuration Model And Solution Procedure

The configuration model used in the current computational investigation is a full-scale F/A-18 aircraft model. The descriptions of the configuration model, the solution procedure, and the computational resources are discussed in the next two sections.

F/A-18 Configuration Model

The basic configuration of the F/A-18 aircraft is modified to include the LEX fences. The grid system and size of the modified configuration is the same as that of the basic configuration for fair comparison. The full F/A-18 aircraft model has an overall length of 17.1 m, a wingspan of 11.4 m, a wing reference area of 37.15 m^2, a wing mean aerodynamic chord of 3.51 m, and a vertical tail reference area of 4.842 m^2. The vertical tail has an aspect ratio of 1.2, a taper ratio of 0.4, and a leading-edge sweep angle of 41.4 deg. The vertical tail has a cantilever angle of 20 deg toward the outboard direction. The fences are placed over the upper surface of the wing LEX, near the intersection with the leading edge of the wing. The surface geometry of the F/A-18 aircraft and the dimensions of the LEX fence are shown in Fig. 1. The fence has a trapezoidal shape with edge angles of 30 deg. The taper ratio of the LEX fence is 0.7, and the thickness of the fence is 0.02 m.

The geometry of the full F/A-18 aircraft is modeled using a structured body-fitted grid system with one-to-one grid connectivity. The grid topology on a cross plane just ahead of the vertical tails is shown in Fig. 2. The grid is a multiblock H–H grid consisting of 53 structured blocks utilizing 2.56 million cells (2.68 million grid points). The global grid extends 5 wing chords upstream and downstream of the aircraft, and 8 wing chords normal to the aircraft. The grid

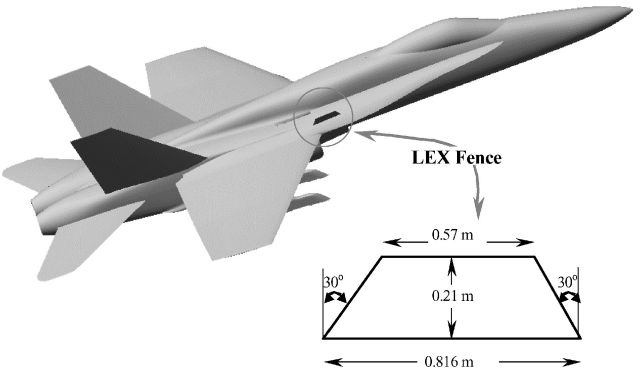

Fig. 1 F/A-18 configuration model and the dimensions of the fence.

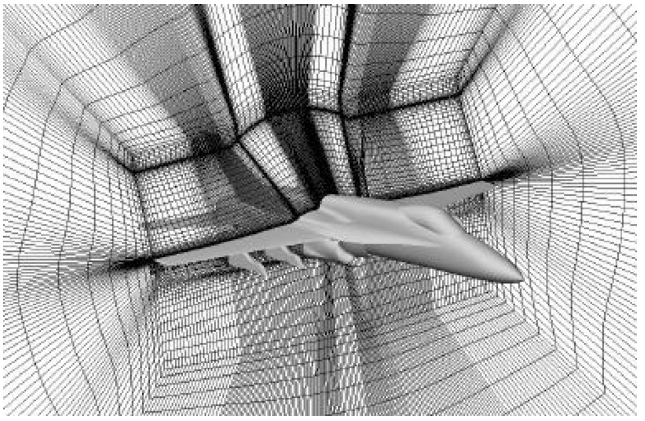

Fig. 2 Grid topology of the crossflow plane.

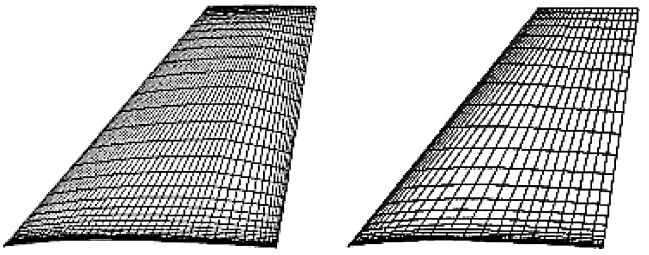

Fig. 3 Vertical tail: a) surface CFD grid and b) CSD grid.

is clustered near the apex and leading edge of the wing LEX to produce robust and well-defined leading-edge vortices.

For the structure dynamics analysis, the vertical tail of the F/A-18 aircraft is modeled using second-order hexahedral elements. The computational structural dynamics (CSD) and computational fluid dynamics (CFD) surface grids of the vertical tail are shown in Fig. 3. The CFD and CSD grids are not identical. A total of 1840 grid cells defined the CFD surface grid of the tail, whereas 576 grid cells defined the CSD surface grid of the tail. The forces and deflections are interpolated between the two grids using the interfacing module outlined before. The material of the vertical tail is assumed to be aluminum and isotropic. Young's modulus of elasticity is 6.896×10^{10} N/m^2, the density is 2765 kg/m^3, and Poisson's ratio is 0.33.

Solution Procedure

This multidisciplinary problem is solved using two steps: The first step solves for the vortical flow characteristics around the rigid configuration. The initial condition of this step is the undistributed freestream condition. The solution is carried out until the changes in the vortical flowfield become insignificant. The second step is time-accurate synchronized computation of the aerodynamic flowfield and the aeroelastic responses of the flexible configuration. The initial

condition of this step is the final solution of the first step. Strong coupling between the fluid dynamics flow and the structural-dynamics response of the vertical tail is considered in this investigation. Strong coupling occurs when the aerodynamic forces of the flowfield are transferred to the solid, and consequently, the inertial effects of the motion of the solid are fed back into the fluid every time step. The inertial effects of the solid are fed back into the fluid in terms of accelerations, velocities, and deflections. The accelerations and velocities are used to update the boundary conditions on the flexible tail surfaces. The deflections are used to modify the CFD grid to accommodate the deformed shape of the vertical tail. The transfer of solution data between the fluid and structure disciplines occurs every time step. The time steps of the computations are fixed in all cases at 10^{-4} s.

The problem is solved on a Linux computer cluster of six units. The total grid is divided between the six processors using domain decomposition. The speed of each processor is 1.0 GHz. Every partition of the grid requires approximately 160 MB of memory. The computational cost is about 40 μs per time step per grid point on the six-unit cluster. Each case presented herein requires about 142 CPU working hours.

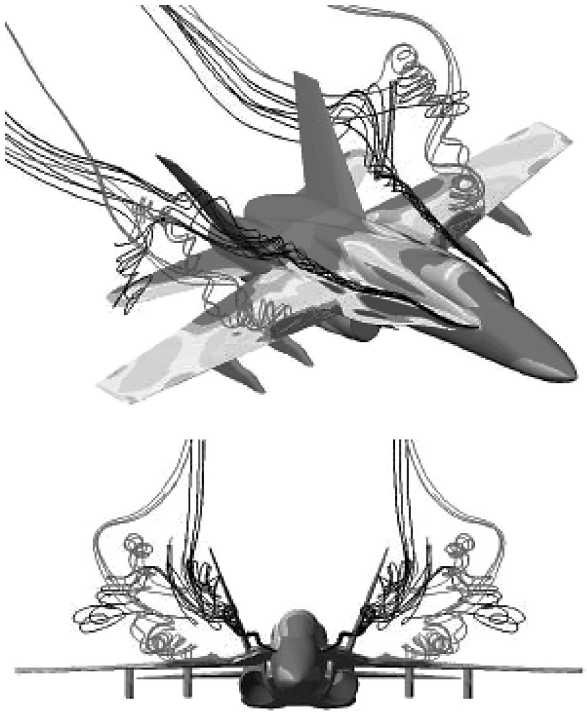

a) Fences off (α = 30 deg)

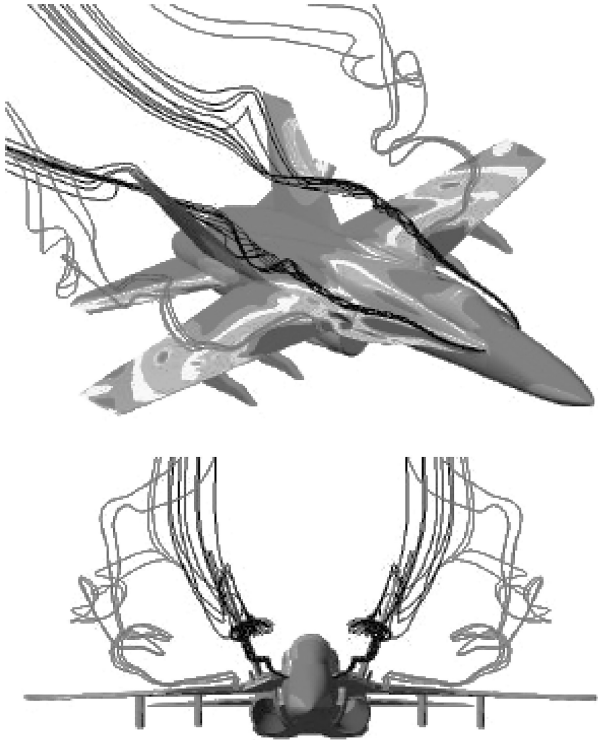

b) Fences on (α = 30 deg)

Fig. 4 Three-dimensional and front view snapshots of the instantaneous streamlines of the LEX and the wing leading edge of the F/A-18 aircraft.

Results and Discussion

The aerodynamic and aeroelastic fields around the full F/A-18 aircraft are analyzed at typical flight conditions. The flight conditions

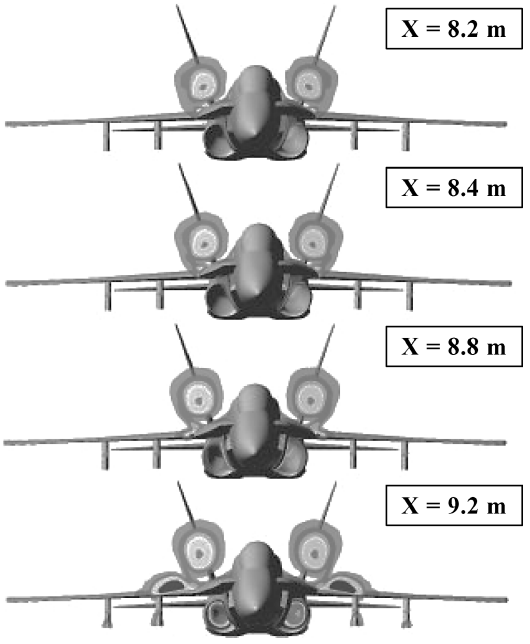

a) Fences off (α = 30 deg)

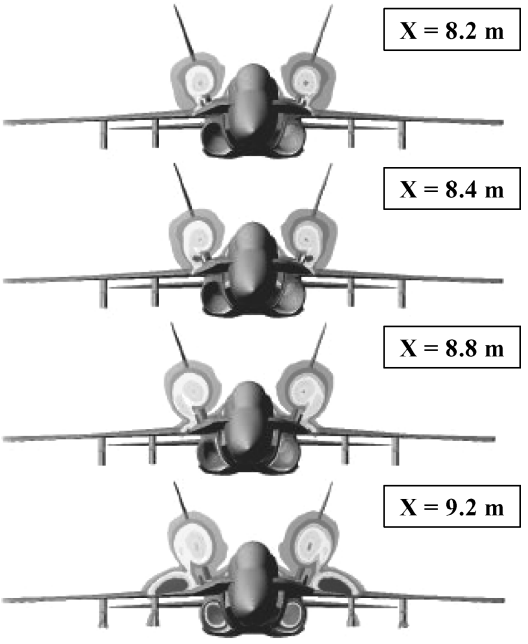

b) Fences on (α = 30 deg)

Fig. 5 Total pressure contours on crossflow planes over the F/A-18 aircraft.

considered herein correspond to the NASA F/A-18 high alpha research vehicle (HARV). The aircraft is pitched over wide range of angles of attack ($\alpha = 25$–40 deg) at a Mach number of 0.243 and a Reynolds number of 11×10^6. The inlet mass flow rate of the engine corresponds to the maximum power condition.

Effects of the LEX Fence on the Aerodynamic Flowfield

The effects of the LEX fence on the aerodynamics flowfield around the F/A-18 aircraft at 30-deg angle of attack are shown in Figs. 4 and 5. Figure 4 shows three-dimensional and front view snapshots of the instantaneous streamlines of the LEX and wing vortices over the F/A-18 aircraft. As the leading-edge vortex travels downstream, the core of the vortex makes an abrupt kink and forms a spiral vortex. The spiral vortex was also observed by Fisher et al.[23] in flight tests of the F/A-18 HARV vehicle. The spiral vortex persists for several turns before bursting. The rotation sense of the spiral vortex is opposite to the direction of rotation of the leading-edge vortex. The fences also delay the onset of vortex bursting. In the fences-off model, most of the vortical flows are outboard of the vertical tails. Figure 4 shows that the fences force the vortical flow to move inward toward the vertical tail. This inward motion balances the loads on both sides of the vertical tail in contrast to the fences-off model.

The total pressure contours on crossflow planes over the F/A-18 aircraft at different longitudinal locations are shown in Fig. 5. Figure 5 shows that, as the vortical flow crosses the fences, the LEX vortex splits into two corotating vortices. Once the vortices pass the

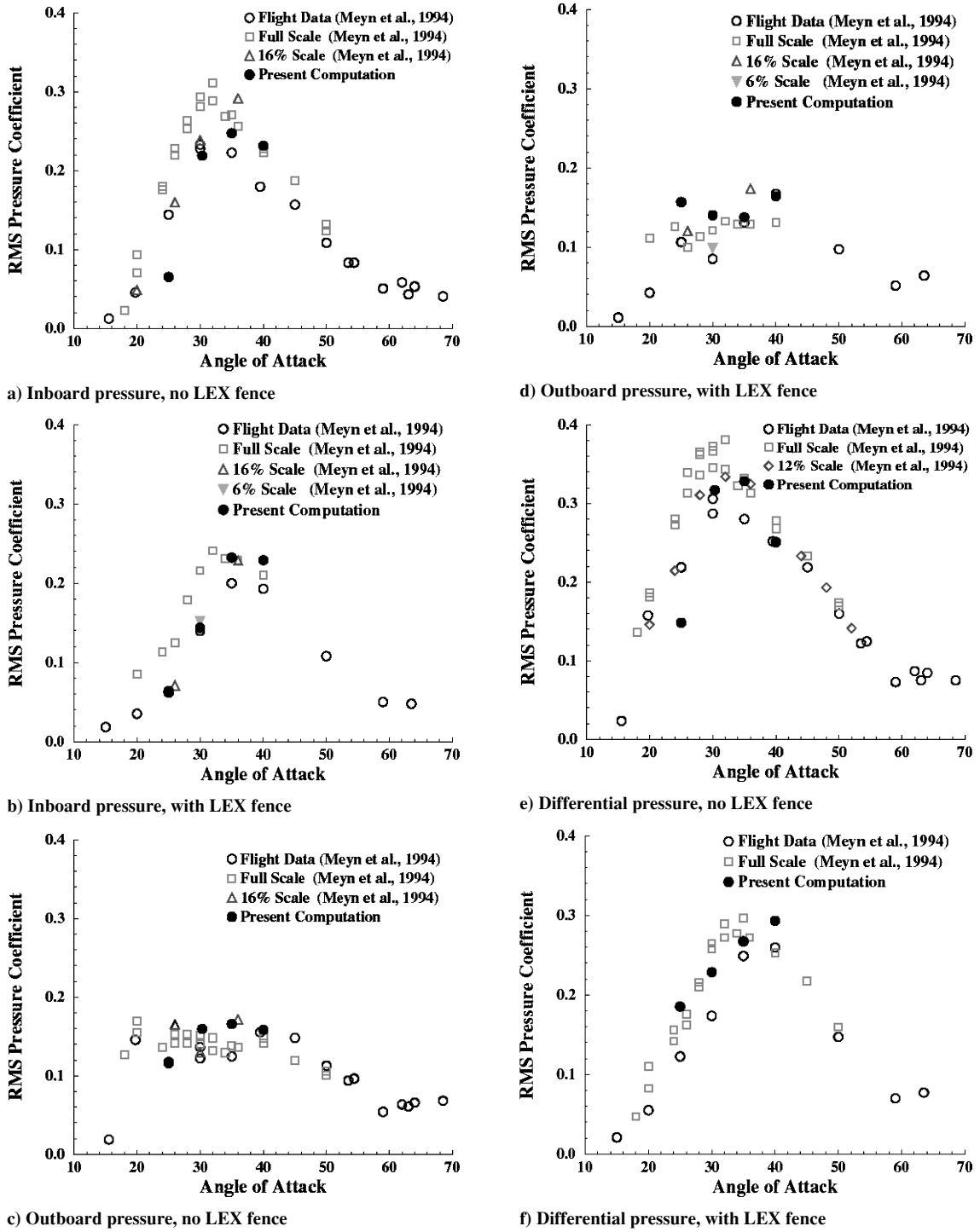

a) Inboard pressure, no LEX fence

b) Inboard pressure, with LEX fence

c) Outboard pressure, no LEX fence

d) Outboard pressure, with LEX fence

e) Differential pressure, no LEX fence

f) Differential pressure, with LEX fence

Fig. 6 At 45% chord and 60% span of the vertical tail, rms pressure coefficient.

fences, they start to move in a spiral path over each other. Thereafter, they merge together, producing a larger vortex. This means that the energy of the vortex is spread over a larger region than that of the basic configuration. The vortex split and merge increases the axial momentum of the LEX vortex, which results in a delay in the vortex breakdown location, as shown in Fig. 4.

Buffet Characteristics at 45% Chord and 60% Span

The results of the point at 45% chord and 60% span of the vertical tail from several wind-tunnel experiments and flight tests have been published by, for example, Shah,[15] Meyn and James,[17] Pettit et al.,[21] Meyn et al.,[24] and James and Meyn.[25] Therefore, the unsteady pressure is monitored and analyzed at this point on both sides of the vertical tail. The effects of the LEX fence on the root mean square (rms) of inboard, outboard, and differential pressure coefficients are shown in Fig. 6. The results are compared with flight-test data, full-, 16, 12, and 6%-scale wind-tunnel data (Meyn et al.[24]). The results compare well with the experimental and flight data for both the fences-off and fences-on configurations. The results clearly show that the LEX fence reduces the rms pressure on the inboard surface of the tail. This, in turn, results in reducing the differential pressure on the vertical tail. For both configurations, the rms pressure of the inboard surface is larger than that of the outboard surface. This indicates that the inboard surface of the vertical tail has a more significant contribution in the unsteadiness of the buffet problem than the outboard surface. The rms pressure of the outboard surface is less sensitive to the angle of attack. The results indicate that the fences-off configuration experiences the maximum peaks between the 30- and 35-deg angle of attack. For the fences-on configuration,

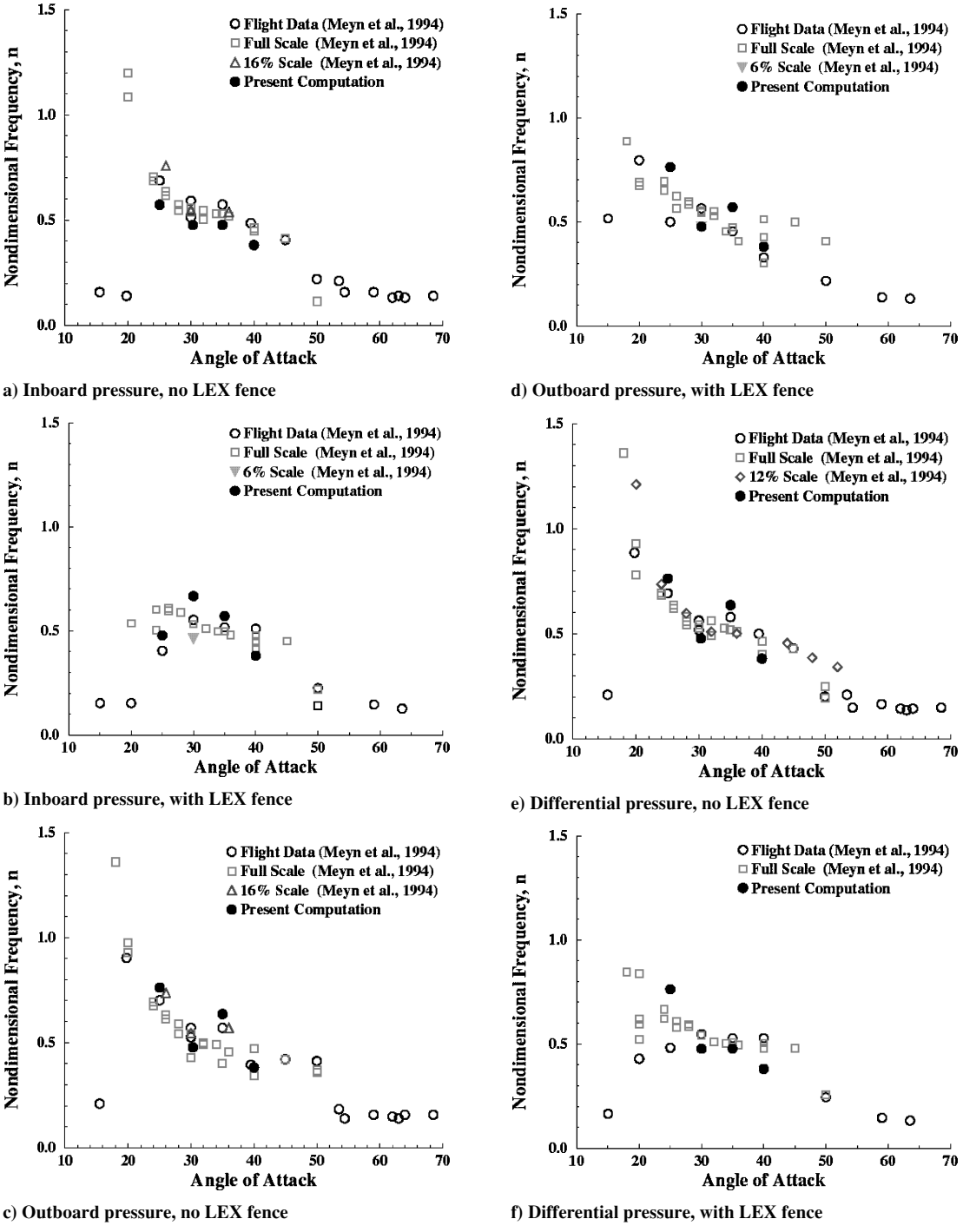

a) Inboard pressure, no LEX fence

b) Inboard pressure, with LEX fence

c) Outboard pressure, no LEX fence

d) Outboard pressure, with LEX fence

e) Differential pressure, no LEX fence

f) Differential pressure, with LEX fence

Fig. 7 Predominant frequencies of the buffet pressure peaks.

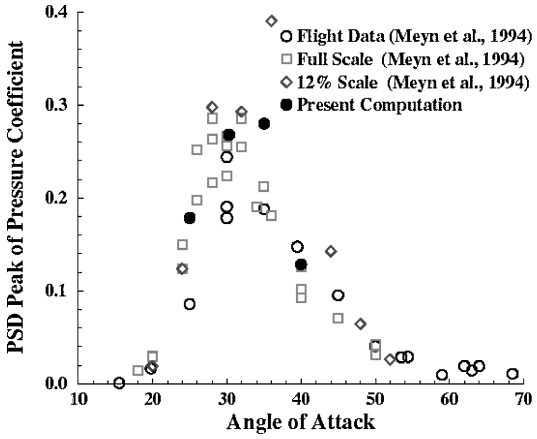

a) No LEX fence

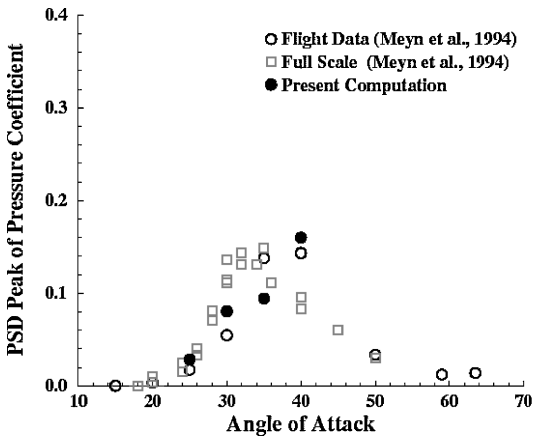

b) With LEX fence

Fig. 8 PSD peaks of the differential pressure coefficient at 45% chord and 60% span.

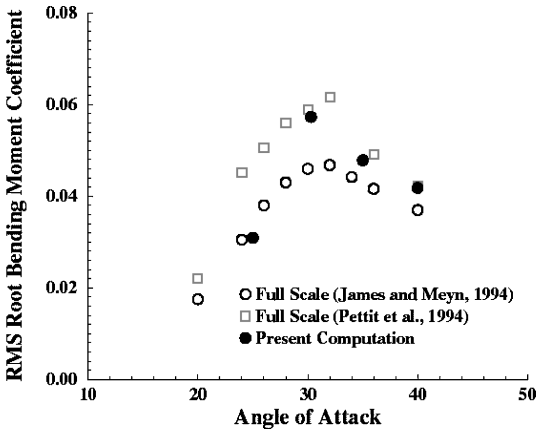

a) No LEX fence

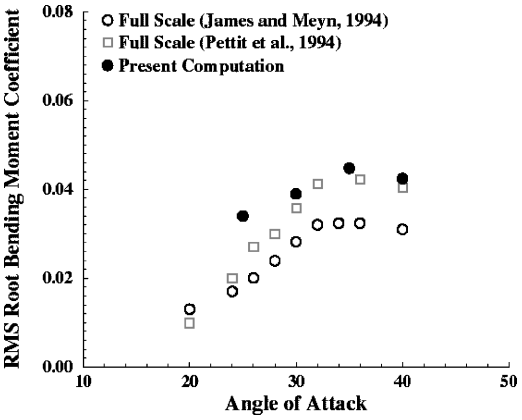

b) With LEX fence

Fig. 9 Tail RBM coefficient rms.

the maximum peaks occur between the 35- and 40-deg angle of attack. This shows that the LEX fence shifts the onset of maximum tail buffet to higher angles of attack, in agreement with the experimental data of James and Meyn.[25]

The buffet excitation spectra of the F/A-18 vertical tail are computed over the angle-of-attack range. The buffet pressure spectra are normalized by the freestream dynamic pressure and are presented as[21] $\sqrt{[nF(n)]}$, where $F(n)$ is the buffet excitation power spectral density (PSD) and n is the nondimensional frequency. The buffet excitation PSD is used to compare the buffet magnitude between the cases considered. The predominant frequencies of the buffet pressure peaks are shown in Fig. 7 for the inboard, outboard, and differential pressures. The results compare well with the flight and wind-tunnel data for both the fences-off and fences-on configuration models. For both configurations, the buffet excitation peaks shift into lower frequencies as the angle of attack increases. The frequency shift at high angles of attack has been observed by several researcher using different models, e.g., Pettit et al.,[21] Meyn et al.,[24] and Washburn et al.[26]

The peaks of the power spectra of the differential pressure coefficient are compared with the flight data and experimental data for the fences-off and fences-on configurations in Fig. 8. The computed results compared well with the flight and experimental data for both configurations. Figure 8 shows that the LEX fence shifts the maximum buffet power into higher angle of attack. The LEX fence reduces the peak power of the differential pressure at all angles of attack except at 40-deg angle of attack, which indicates that the effectiveness of the LEX fences reduces at higher angles of attack.

Root Bending Moment of the Vertical Tail

The root bending moment (RBM) is computed by integrating the differential pressure on the vertical tail. The unsteady pressure is monitored on both sides of the tail at 16 selected transducers locations. The locations of the transducers are similar to those chosen by Meyn et al.[24] The surface pressure surrounding the pressure transducer is assumed to be constant. The loads are assumed to act on the centroid of each area surrounding the transducers. The moment arm is measured from each cell centroid to the tail root.

The rms of the tail root bending moment coefficient for the fences-off and fences-on configurations is shown in Fig. 9. The results are compared with the full-scale wind-tunnel data of Pettit et al.[21] and James and Meyn.[25] The experimental data were obtained using different sensor densities and slightly different model setup. Pettit et al.[21] used a 6×6 transducer array, whereas James and Meyn[25] used a 6×8 transducer array. James and Meyn[25] showed that the density of the transducers array affects the integration of the buffet loads on the vertical tail. The results compare well with the experimental data over the angle-of-attack range for both configurations. The LEX fence configuration produces maximum RBM at an angle of attack of 35 deg in contrast to the basic configuration, where maximum RBM occurs at an angle of attack of 30 deg. This emphasizes the conclusion that the LEX fences shift the maximum buffet conditions into higher angles of attack. Figure 9 also shows that the LEX fence reduces the RBM at all angles of attack except at 40 deg, which emphasizes the conclusion of the preceding section that the effectiveness of the LEX fence reduces at higher angles of attack. This conclusion is in agreement with the experimental observations of Shah.[15]

Aeroelastic Responses

The time histories of the normal deflection at the leading-edge and trailing-edge points of the vertical tail tip are shown in Fig. 10. Figure 10 shows the results for both the fences-off and fences-on configurations at 30-deg angle of attack. Figure 10 shows that the fences reduced the amplitude of deflection at both edges. The

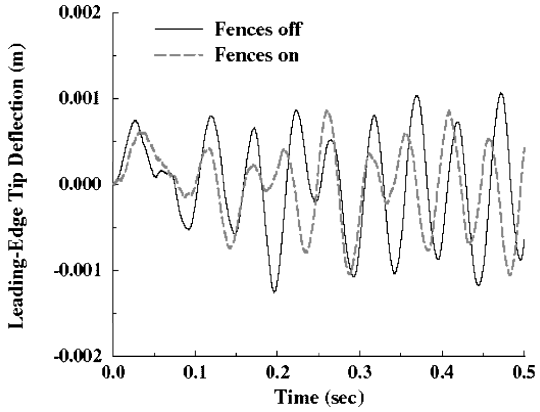

a)

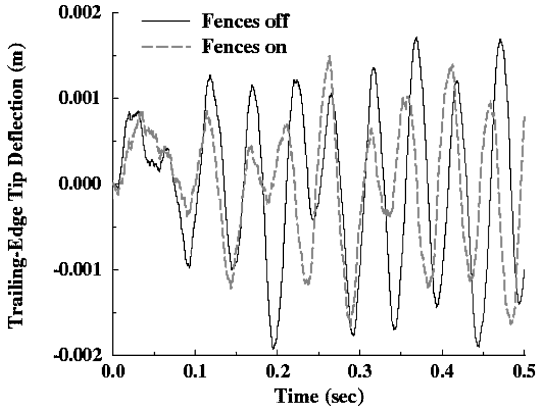

b)

Fig. 10 Normal deflection of leading edge and trailing edge of the vertical tail tip.

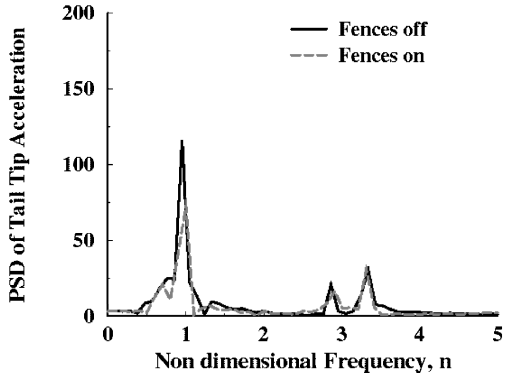

a) Leading edge

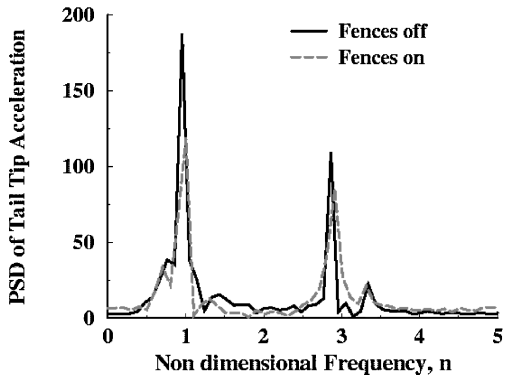

b) Trailing edge

Fig. 11 PSD of the tail tip acceleration of the vertical tail.

different amplitude of deflection between the leading edge and trailing edge of the vertical tail are indication of the torsional deformation of the vertical tail. Figure 10 also shows that the presence of the LEX fence caused a slight increase in the frequency of the tail deflections.

The PSD of the tail tip acceleration of the vertical tail is shown in Fig. 11 for the leading-edge and trailing-edge points. The PSD is computed using MATLAB® toolbox. The PSD is computed based on a time span of $\frac{1}{2}$ s corresponding to 5000 sample points. The actual frequencies of the power peaks may be missed because of the small number of sample points. Therefore, several values of frequency interval are used to extract more accurate frequencies from the accelerations spectra. Figure 11 shows a slight increase in the frequencies of the power peaks caused by the presence of the LEX fence. This increase in the dominant frequencies is consistent with the results of Fig. 10. The predominant nondimensional frequency of the tail tip acceleration is about 1.0, which agrees with the experimental value reported by Pettit et al.[21] The first two peaks occur around the nondimensional frequencies of 1 and 3, corresponding to the first bending and first torsion modes. The first peak is significantly higher than the second peak, which indicates the dominance of the first bending mode. A third peak occurs at the second bending mode but with smaller level than the peaks at the first bending mode. Figure 11 shows that the LEX fence reduces the acceleration powers at both the leading and trailing edge points. At the leading edge point, the acceleration power has a 38% reduction for the first bending mode and 22% for the first torsion mode. At the trailing-edge point, the acceleration power has a 36% reduction for the first bending mode and 21% for the first torsion mode. Figure 11 also shows that the trailing edge of the vertical tail experiences higher acceleration power than the leading edge in agreement with the flight and wind-tunnel results reported by Bean and Lee.[7]

Conclusions

A high-fidelity multidisciplinary computational investigation for prediction and alleviation of the buffet characteristics of the vertical tail of F/A-18 aircraft is presented. Alleviation of vertical tail buffeting is achieved using LEX fences. The computational results are in close agreement with several flight and wind-tunnel data over a wide range of high angles of attack. The LEX fences shift the onset of maximum buffet condition to higher angle of attack. The LEX fences were effective in reducing the rms of differential pressure, the rms of RBM, and the amplitude of deflections of the vertical tail. The acceleration powers of the vertical tail tip are reduced by up to 38% at 30-deg angle of attack. However, the effectiveness of the LEX fences for buffet alleviation is reduced for very high angles of attack.

Acknowledgments

This research work is supported by the U.S. Air Force Research Laboratory. The author wishes to acknowledge the Technical Monitor, Lawrence J. Huttsell, for valuable discussions. Vincent Harrand and Mark Underwood of CFD Research Corporation provided invaluable support during this study.

References

[1]Wentz, W. H., "Vortex–Fin Interaction on a Fighter Aircraft," AIAA Paper 87-2474-CP, Aug. 1987, pp. 392–399.

[2]Sellers, W. L., III, Meyers, J. F., and Hepner, T. E., "LDV Survey Over a Fighter Model at Moderate to High Angle of Attack," Society of Automotive Engineers, SAE Paper 88-1448, Oct. 1988.

[3]Lee, B., and Brown, D., "Wind Tunnel Studies of F/A-18 Tail Buffet," *Journal of Aircraft*, Vol. 29, No. 1, 1992, pp. 146–152; also AIAA Paper 90-1432, June 1990.

[4]Cole, S. R., Moss, S. W., and Dogget, R. V., Jr., "Some Buffet Response Characteristics of a Twin-Vertical-Tail Configuration," NASA TM 102749, Oct. 1990.

[5]Martin, C. A., and Thompson, D. H., "Scale Model Measurements of Fin Buffet due to Vortex Bursting on F/A-18," Manoeuvering Aerodynamics, AGARD, CP 497, May 1991.

[6]Moses, R. W., and Pendleton, E., "A Comparison of Pressure Measurements Between a Full-Scale and a 1/6-Scale F/A-18 Twin Tail During Buffet," NASA TM 110282, Aug. 1996.
[7]Bean, D. E., and Lee, B. H. K., "Correlation of Wind Tunnel and Flight Test Data for F/A-18 Vertical Tail Buffet," AIAA Paper 94-1800, April 1994.
[8]Moses, R. W., and Huttsell, L. J., "Fin Buffeting Features of an Early F-22 Model," AIAA Paper 2000-1695, April 2000.
[9]Rizk, Y., Guruswamy, G., and Gee, K., "Numerical Investigation of Tail Buffet on F-18 Aircraft," AIAA Paper 92-2673-CP, June 1992, pp. 573–587.
[10]Rizk, Y., Guruswamy, G., and Gee, K., "Computational Study of F-18 Vortex Induced Tail Buffet," AIAA Paper 92-4699, Sept. 1992.
[11]Gee, K., Murman, S., and Schiff, L., "Computational Analysis of F/A-18 Tail Buffet," AIAA Paper 95-3440-CP, Aug. 1995, pp. 151–162; also "Computation of F/A-18 Tail Buffet," *Journal of Aircraft*, Vol. 33, No. 6, 1996, pp. 1181–1189.
[12]Sheta, E. F., Stacey, S. G., and Huttsell, L. J., "Characteristics of Vertical Tail Buffet of F/A-18 Aircraft," AIAA Paper 2001-0710, Jan. 2001.
[13]Sheta, E. F., and Huttsell, L. J., "Numerical Analysis of F/A-18 Vertical Tail Buffeting," AIAA Paper 2001-1664, April 2001.
[14]Rao, D., Puram, C., and Shah, G., "Vortex Control for Tail Buffet Alleviation on a Twin-Tail Fighter Configuration," Society of Automotive Engineers, SAE Paper 892221, Sept. 1989.
[15]Shah, G. H., "Wind-Tunnel Investigation of Aerodynamic and Tail Buffet Characteristics of Leading-Edge Extension Modifications to the F/A-18," AIAA Paper 91-2889-CP, Aug. 1991, pp. 395–412.
[16]Lee, B., Brown, D., Zgela, M., and Poirel, D., "Wind Tunnel Investigation of Tail Buffet on the F-18 Aircraft," Aircraft Dynamic Loads Due to Flow Separation, AGARD, CP 483, Sept. 1990.
[17]Meyn, L. A., and James, K. D., "Full Scale Wind Tunnel Studies of F/A-18 Tail Buffet," *Journal of Aircraft*, Vol. 33, No. 3, 1996, pp. 589–595; also AIAA Paper 93-3519, Aug. 1993.
[18]Lee, B., and Valerio, N., "Vortical Flow Structure near the F/A-18 LEX at High Incidence," *Journal of Aircraft*, Vol. 31, No. 5, 1994, pp. 1221–1223.
[19]Kingsley, G. M., Siegel, J. M., Harrand, V. J., Lawrence, C., and Luker, J., "Development of the Multi-Disciplinary Computing Environment (MDICE)," AIAA Paper 98-4738, Sept. 1998.
[20]Sheta, E. F., "Computational Investigation and Validation of Twin-Tail Buffet Response Including Dynamics and Control," Ph.D. Dissertation, Old Dominion Univ., Norfolk, VA, May 1998.
[21]Pettit, C., Brown, D., and Pendleton, E., "Wind Tunnel Tests of Full-Scale F/A-18 Twin Tail Buffet: A Summary of Pressure and Response Measurements," AIAA Paper 94-3476-CP, Aug. 1994, pp. 207–218.
[22]Brown, S. A., "Displacement Extrapolation for CFD and CSM Analysis," AIAA Paper 97-1090, April 1997.
[23]Fisher, D. F., Del Frate, J. H., and Richwine, D., "In-Flight Flow Visualization Characteristics of the NASA F-18 High Alpha Research Vehicle at High Angles of Attack," NASA TM 4193, May 1990.
[24]Meyn, L. A., James, K. D., and Geenen, R. J., "Correlation of F/A-18 Tail Buffet Results," High Alpha Projects and Technology Conf., Dryden Flight Research Center, Edward, CA, July 1994.
[25]James, K. D., and Meyn, L. A., "Dependence of Integrated Vertical-Tail Buffet Loads for F/A-18 on Sensor Density," Society of Automotive Engineers, SAE Paper 941140, April 1994.
[26]Washburn, A. E., Jenkins, L. N., and Ferman, M. A., "Experimental Investigation of Vortex–Fin Interaction," AIAA Paper 93-0050, Jan. 1993.